JOURNAL OF MATERIALS SCIENCE 27 (1992) 423–428

Creep rupture studies of two alumina-based ceramic fibres

D. J. PYSHER, R. E. TRESSLER
Center for Advanced Materials, The Pennsylvania State University, University Park, PA 16802, USA

Creep rupture tests were performed in air on two polycrystalline oxide fibres (Al_2O_3, Al_2O_3–ZrO_2) using both filament bundles and single filaments. Tests were performed at applied stresses ranging from 50–150 MPa over the temperature range 1150–1250 °C. Under these conditions, creep rates for the alumina–zirconia fibre ranged from 4.12×10^{-8}–7.70×10^{-6} s^{-1}. At a given applied stress, at 1200 °C, creep rates for the alumina fibre were 2–10 times greater than those of the alumina–zirconia fibre. Stress exponents for both fibres ranged from 1.2–2.8, while the apparent activation energy for creep of bundles of the alumina–zirconia fibre was determined to be 648 ± 100 kJ mol^{-1}. For the alumina–zirconia fibre, the two test methods yielded similar steady-state creep rates, but the rupture times were generally found to be longer for bundles than for single filaments. The steady-state creep behaviour of these alumina-based fibres is consistent with an interface-reaction-controlled diffusion-controlling mechanism.

1. Introduction

Under certain conditions, the high-temperature creep and rupture behaviour of fibre-reinforced composites is controlled by the creep and rupture behaviour of their constituent fibres. Creep rupture investigations of ceramic fibres have been limited [1–6]. Difficulties in developing accurate and reliable test methods (in particular, methods for creep strain measurement) have impeded the collection of creep rupture data for currently available small-diameter fibres. In addition, previous investigations have failed to present a complete description of the processes that govern the creep and rupture of such fibres because microstructural evaluations to substantiate proposed creep mechanisms and rupture processes have not been reported.

The objectives of this work were (i) to develop an accurate and reliable test method for evaluating the creep rupture behaviour of ceramic fibres, and (ii) to investigate the creep rupture behaviour of two currently available alumina-based fibres with potential as reinforcement for metal–, intermetallic–, and ceramic–matrix composites. In this paper, results from initial creep rupture investigations of a polycrystalline alumina fibre and a two-phase alumina–zirconia fibre (Fibre FP and PRD-166) are reported.* Characterization of the microstructural evolution prior to creep rupture and the effect of the second-phase ZrO_2 on creep and rupture behaviour will be more thoroughly discussed in a subsequent paper.

2. Experimental procedure

Both fibres were received on spools in the form of bundles containing approximately 200 filaments each without any organic sizing or coating (Type I fibres). A summary of fibre characteristics is given in Table I. Elemental analyses are semi-quantitative and were obtained via emission spectroscopy analysis. Other data were obtained from Romine [7]. Scanning electron micrographs of as-received fibres are shown in

TABLE I Polycrystalline Al_2O_3-based fibre properties

	Fibre FP	PRD-166	Reference
Composition (wt %)	> 99% α-Al_2O_3	α-Al_2O_3, ≈ 20% tet. ZrO_2	[7]
Density (g cm^{-3})	3.92	4.20	[7]
Average grain size (μm)	0.5	Al_2O_3 0.5, ZrO_2 0.1	[7]
Diameter (μm)	20	20	[7]
Strength (GPa)[a]	1.38	2.10	[7]
Elastic modulus (GPa)[b]	380	380	[7]
Major elements (> 0.1%)	Mg (0.5%)	Y (0.5%–5%)	Present work
Minor elements (0.01–0.1%)	Si, Ca, Zr, Fe	Si, Ca, Mg, Ti, Fe	Present work

[a] 0.64 cm gauge length.
[b] 25.0 cm gauge length.

*The fibres were manufactured by E. I. Du Pont de Nemaurs & Co., Wilmington, DE, USA.

0022–2461/92 $03.00 + .12

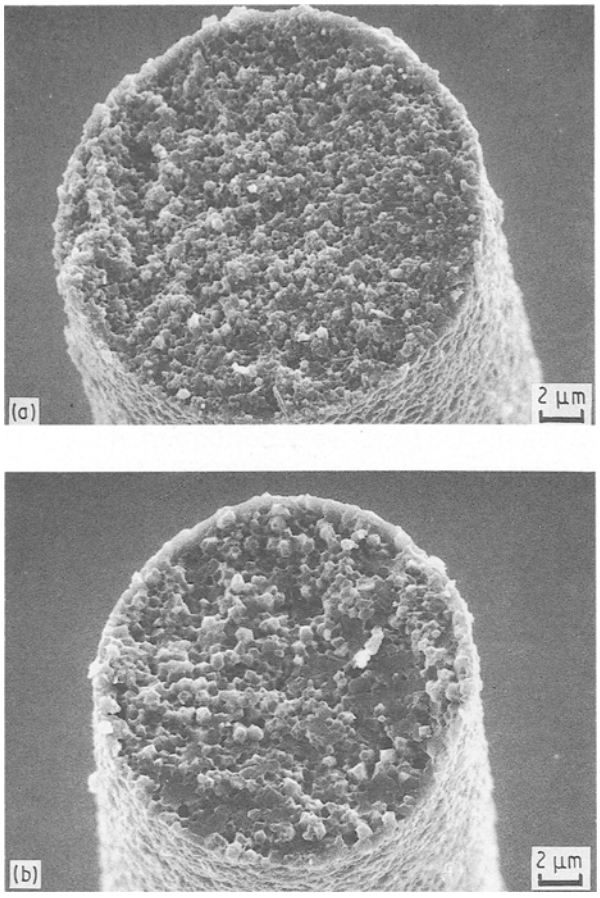

Figure 1 Scanning electron micrographs of (a) PRD-166 and (b) fibre FP.

Fig. 1. Creep rupture tests were performed using both bundles and single filaments. Different techniques were used to measure creep strain for each of the sample geometries.

2.1. Test specimens

Creep rupture test specimens of bundles were fabricated by epoxying both ends of a bundle of fibres, ≈ 61 cm long, into hypodermic needles. A small eyelet screw, from which the applied load was suspended, was epoxyed to one of the hypodermic needles. Targets, for use in measuring fibre displacement, were cut from 50 μm thick platinum foil, folded in half, and attached to the bundle with a small amount of mullite gel to mark the gauge section of the bundle creep sample. Care was taken to ensure that edges of both flags closest to the gauge section remained perpendicular to the fibre bundle. A nominal distance of 2.54 cm separated the targets. The mullite gel, made from fumed Al_2O_3 (aluminium oxide C) and SiO_2 (Aerosil 200) powders and deionized water using a method similar to that described by Ghate *et al.* [8], was also used to coat the portions of the bundle outside the gauge section, forming a single-bundle composite. A schematic illustration of the bundle test specimen is shown in Fig. 2.

Single-filament creep rupture test specimens were fabricated by epoxying single filaments, which were extracted from the as-received bundles, to two manila tabs. The filaments were aligned along the centre line of the tabs, collinear with the prepunched holes in both tabs. The tab-to-tab sample length was ≈ 35 cm. A schematic drawing of the single-filament test specimen is shown in Fig. 3.

2.2. Test apparatus

Creep rupture specimens fabricated from bundles were tested using the apparatus shown in Fig. 2. After lowering a specimen through the furnace, the upper hypodermic needle on the specimen was placed in a pivot bearing seated in the upper mount of the creep frame. The specimen was then rotated so that the platinum targets were perpendicular to the light path between the halogen light source and the electro-optical extensometer (Model 200-X-2, Zimmer OHG). After heating the furnace, 25 °C min^{-1}, and stabilizing at the test temperature, the dead load was suspended from the specimen via a swivel and hook from the eyelet epoxyed to the bottom of the fibre bundle. The relative displacement of the two platinum targets was monitored using the extensometer and the (voltage) signal was recorded using a stripchart recorder. From the displacement versus time curve, creep strain of the bundle was calculated by dividing the relative target displacement by the initial distance between the targets, i.e. the initial gauge length, l_0, which was measured optically to $\pm$ 5 μm using a Gaertner scientific travelling telescope. Temperature was monitored throughout the test using an S-type thermocouple placed near the top of the gauge section of the bundle.

Creep rupture specimens fabricated from single filaments were tested using the apparatus shown in Fig. 3. Specimens were lowered through the furnace and suspended from a hook rigidly attached to the creep frame. Care was taken to align the test specimen with both the loading hook and the core of the super linear variable capacitor (SLVC) transducer (Model 1082, Automatic Systems Laboratories). After heating the furnace to temperature, 25 °C min^{-1}, and allowing 5 min for stabilization, the loading hook was placed on the bottom tab and the dead load was applied. Filament displacement was measured using the SLVC and was recorded on a stripchart recorder. Creep strain of the filament was calculated by dividing the overall measured displacement by the gauge length of the filament, approximated by the length of the hot zone of the furnace (that length of the furnace in which the temperature was within 50 °C of the maximum furnace temperature). Temperature was monitored throughout the test using an S-type thermocouple placed near the centre of the furnace, within close proximity to the test filament.

Determination of the applied stress for both of the test specimens used in this investigation was performed after rupture of the specimen. The applied stress for the bundle specimen geometry was calculated from the weight of the loading train below the gauge section and from the cross-sectional area of the fibre bundle, determined from the number of filaments in the bundle and the average fibre area (calculated from the measured diameters of at least 20 fibres within the bundle).

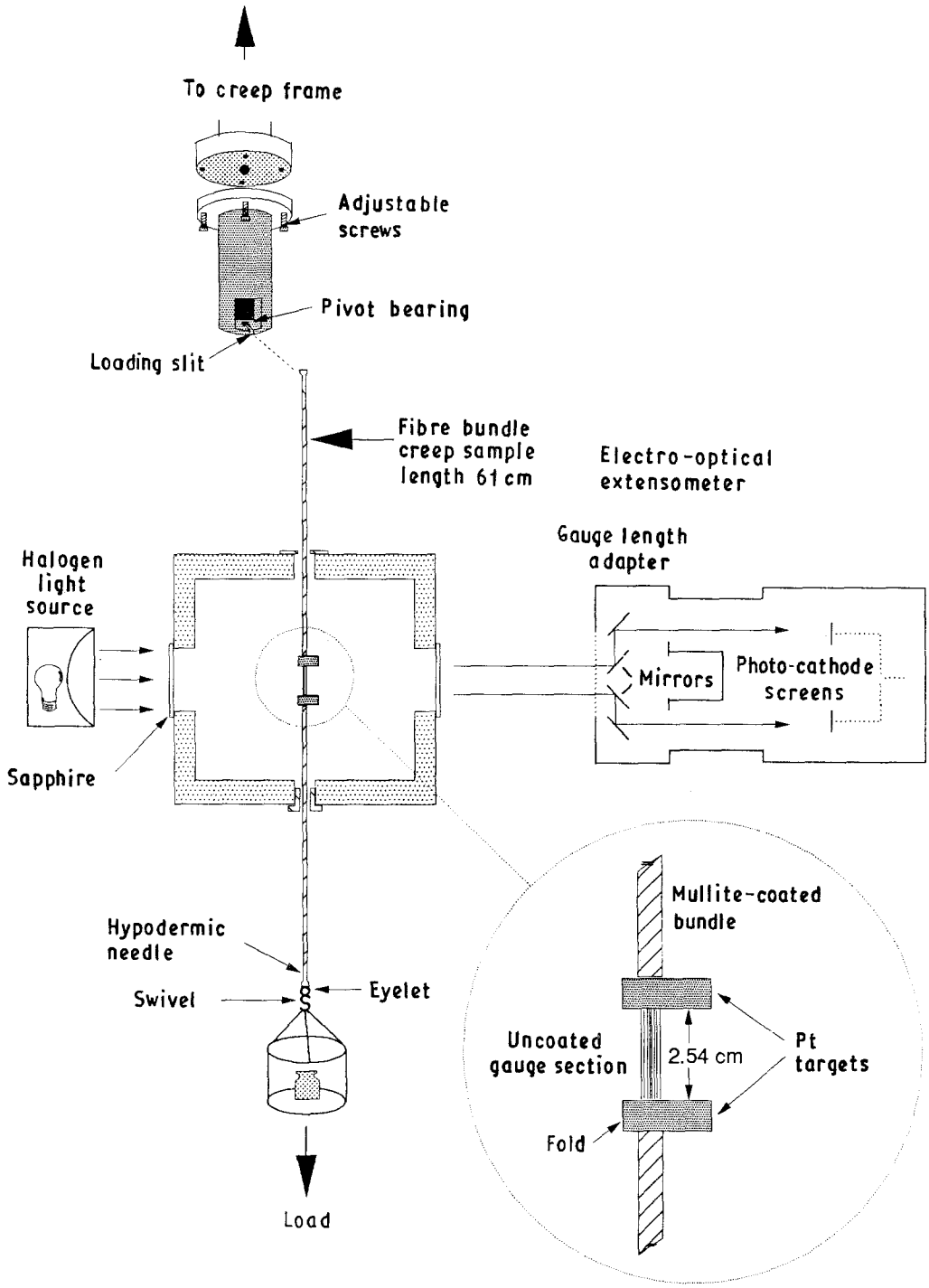

Figure 2 Schematic illustration of the bundle creep rupture sample and test apparatus.

Applied stress for the single filament specimen geometry was calculated using the weight of the applied load plus the bottom mounting tab and from the cross-sectional area of the filament. Filament area was calculated using the diameter of the fracture surface of each test fibre (obtained from scanning electron micrographs).

3. Results

Creep curves for bundle specimens of PRD-166 and Fibre FP, tested at 1200 °C, are shown in Figs 4 and 5, respectively. Creep curves from the bundle tests of both fibres exhibited all three characteristic regions (primary, secondary or steady-state, and tertiary) at all three levels of applied stress, σ_{app}. For both fibre types, steady-state creep rate, $\dot{\varepsilon}_{ss}$, given by the slope of the linear portion of the creep curve, increased with increasing σ_{app}. For the alumina–zirconia fibre, time-to-failure, t_f, and strain-to-failure, ε_f, decreased with increasing σ_{app}. For the alumina fibre, time-to-failure generally decreased with increasing σ_{app} while no clear relationship was evident between ε_f and σ_{app}.

Creep curves for single filament specimens of PRD-166, tested at 1200 °C, are shown in Fig. 6a and b ((b) is an enlarged portion of (a), showing more clearly the creep curves at higher applied stress). In comparison with Fig. 4, note that strains to failure are, in general,

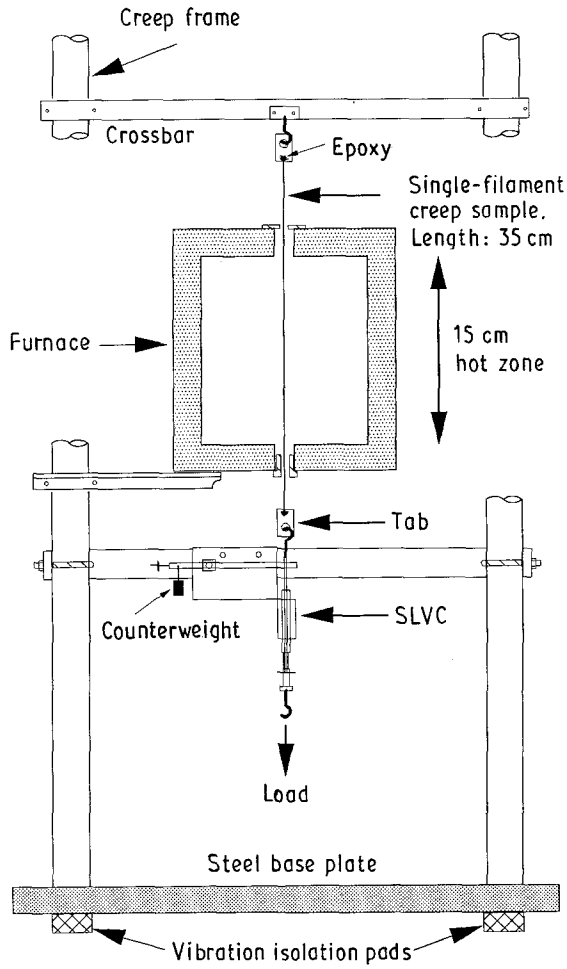

Figure 3 Schematic drawing of the single filament creep rupture sample and test apparatus.

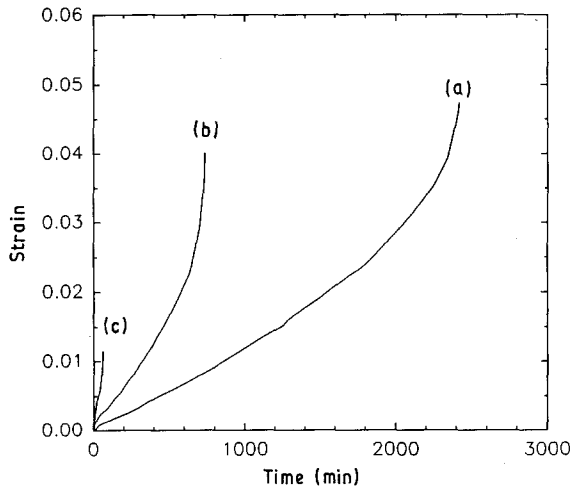

Figure 4 Creep curves for bundles of PRD-166 tested at 1200 °C. σ_{app} = (a) 53, (b) 103, (c) 152 MPa.

lower for the single filament samples than for the bundle samples. As with the bundle samples, both $\dot{\varepsilon}_f$ and t_f tend to decrease with increasing σ_{app}.

The steady-state creep results from tests performed using bundles of PRD-166 and Fibre FP are summarized as $\dot{\varepsilon}_{ss}$ versus σ_{app} (Dorn) plots in Fig. 7, while results from tests performed using single filaments of PRD-166 are shown in Fig. 8. The stress exponents, n, are given by the slopes of least squares regression lines.

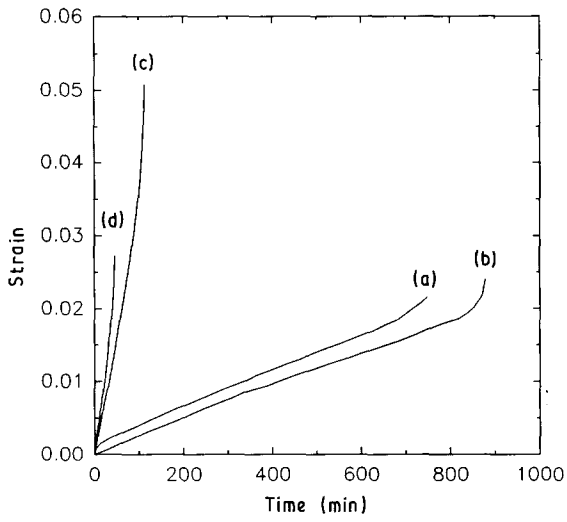

Figure 5 Creep curves for bundles of fibre FP tested at 1200 °C. σ_{app} = (a) 50, (b) 53, (c) 103, (d) 152.

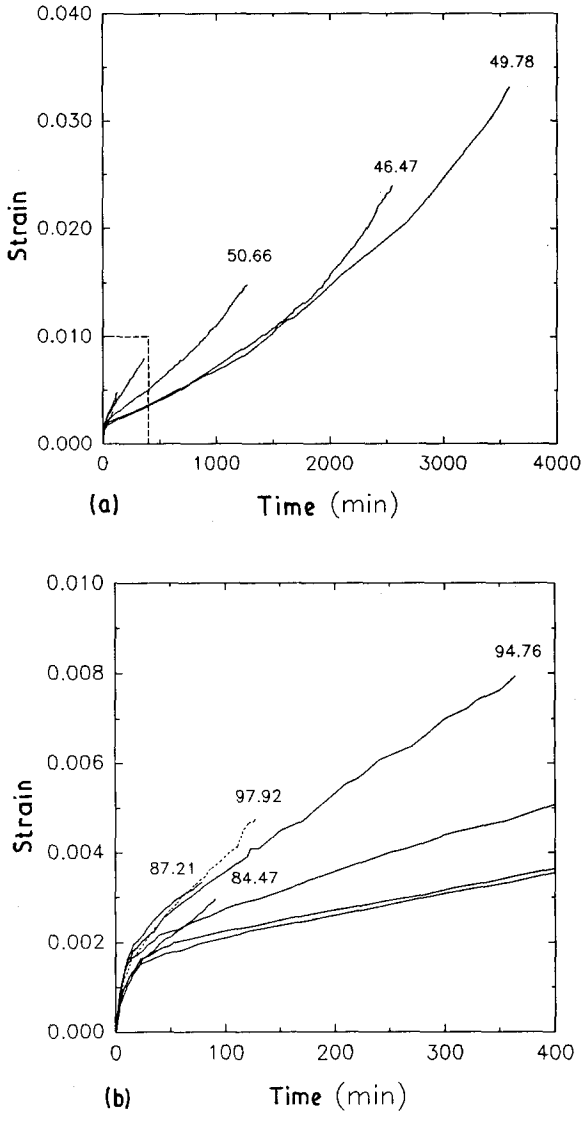

Figure 6 Creep curves for single filaments of PRD-166 tested at 1200 °C. Numbers above curves indicate σ_{app} in MPa. (b) is an enlarged portion of (a), showing more clearly the creep curves at higher applied stresses.

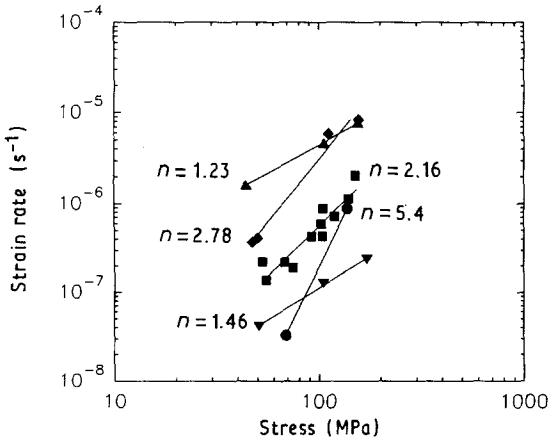

Figure 7 Dorn plot of steady-state creep rate versus applied stress for bundle creep tests. Stress exponents for creep, n, indicate slopes of lines. (▲) PRD-166, 1250°C; (■) PRD-166, 1200°C; (▼) PRD-166, 1150°C; (◆) Fibre FP, 1200°C; (●) NEXTEL 480, 1200°C [4].

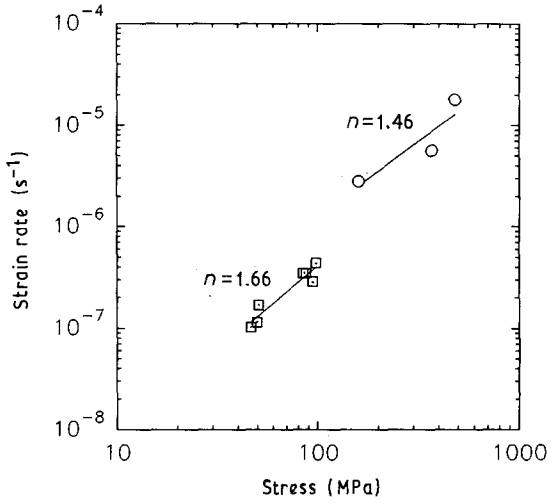

Figure 8 Dorn plot of steady-state creep rate versus applied stress for single filament creep tests. Stress exponents for creep, n, indicate slopes of lines. (○) Sumitomo, 1150°C [9]; (⊡) PRD-166, 1200°C.

Under the present test conditions, n values ranged from ~ 1.25 to ~ 2.15 for the PRD-166 fibre while the stress exponent for fibre FP was found to be ≈ 2.75. For comparative purposes, creep data for two alumina–silica fibres, Nextel® 480 [4] and Sumitomo [9] (both fibres contain a glass phase), are also shown in Figs 7 and 8, respectively. By comparing the bundle data at 1200 °C for PRD-166 with that of fibre FP, it can be seen that, for a given σ_{app}, the Al_2O_3–ZrO_2 fibre exhibits a creep rate that is 2–10 times less than that of the pure Al_2O_3 fibre.

The apparent activation energy, Q_c, can be determined by plotting creep data as $\dot{\varepsilon}_{ss}$ versus inverse temperature, T (at a constant σ_{app}). Data obtained from temperature change tests on bundle specimens of PRD-166 are shown in Fig. 9. At an applied stress of 100 MPa, Q_c was found to be 648 ± 100 kJ mol^{-1}.

Creep rupture data from tests performed using both bundles and single filaments are plotted as $\dot{\varepsilon}_{ss}$ versus t_f in Fig. 10. The lines represent least squares regression of bundle data (——) and single filament data (- - -) obtained from PRD-166 fibres tested at 1200 °C.

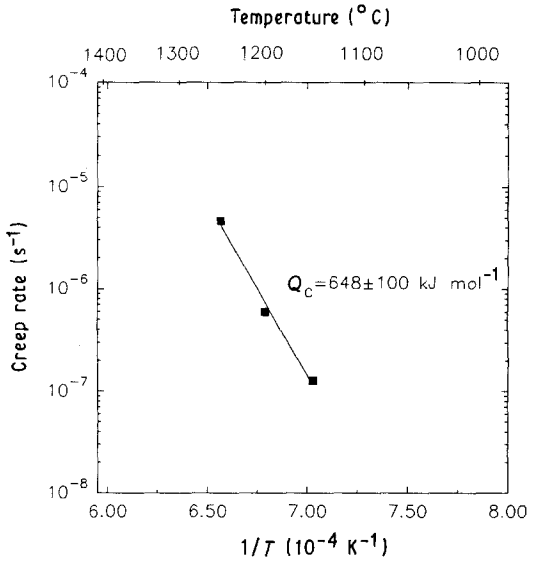

Figure 9 Arrhenius plot of steady-state creep rate versus 1/T. Apparent activation energy for creep, Q_c, determined from least squares regression analysis. (Limits indicate 95% confidence interval.)

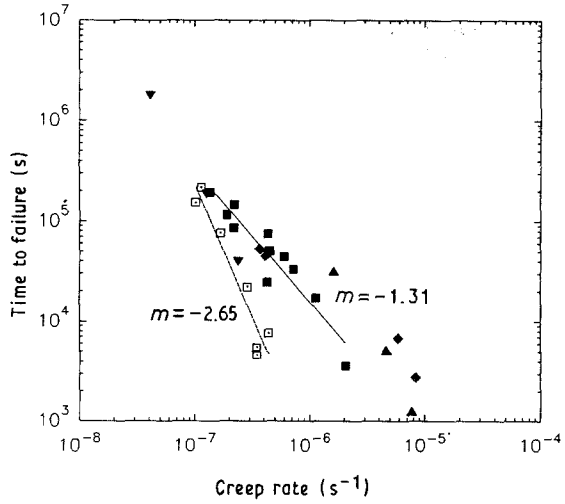

Figure 10 Monkman-Grant plot of time-to-failure versus steady-state creep rate. Slopes of lines, indicated by m, from least squares regression of bundle data (——) and single-filament data (- - -) obtained from PRD-166 tested at 1200 °C. (▲) PRD-166, 1250°C; (■) PRD-166, 1200°C; (▼) PRD-166, 1150°C; (◆) Fibre FP, 1200°C; (⊡) PRD-166, 1200°C; Single filament.

4. Discussion

In general, the creep curves obtained from tests of bundle specimens exhibit a distinct tertiary region (of increasing creep rate with creep strain) while creep curves from single filament specimens tested at lower applied stress (~ 50 MPa) indicate a gradually increasing rate. Although creep damage (cavitation) may explain this observation, it is possible that, for the bundle specimens, the tertiary region is due to an increase in the effective applied stress, resulting from progressive rupture of individual filaments within the bundle.

Constitutive relations such as a power law or Dorn relationship have been used to relate $\dot{\varepsilon}_{ss}$ to applied stress, σ_{app}, grain size, d, and temperature, T. A typical form of the Dorn equation is given by [10]

$$\dot{\varepsilon}_{ss} = \frac{ADGb}{kT}\left(\frac{b}{d}\right)^p\left(\frac{\sigma_{app}}{G}\right)^n \quad (1)$$

where A is a dimensionless constant, D is the appropriate diffusion coefficient, G is the shear modulus, $\boldsymbol{b}$ is the Burger's vector, p is the inverse grain size exponent, n is the stress exponent, k is Boltzmann's constant and T is absolute temperature. The diffusion coefficient, D, is given by

$$D = D_0 \exp\left(\frac{-Q_c}{RT}\right) \quad (2)$$

where D_0 is a frequency factor, Q_c is the apparent activation energy for creep, and R is the gas constant ($8.314\,\mathrm{J\,mol^{-1}\,K^{-1}}$).

Values for p, n and Q_c may be obtained experimentally and used to infer a rate-controlling mechanism(s) for creep, by comparison with theoretical analyses. Although values for n and Q_c given above are only preliminary, (owing to the rather limited range of applied stress and temperature over which data were obtained), they are in agreement with values reported by others from creep investigations of similar fine-grained alumina [11] and alumina–zirconia [12] materials in which the mechanism controlling creep was deduced to be interface-reaction-controlled (IRC) diffusional (Coble) creep.

In order to establish if the mechanism controlling creep in these materials is IRC, tests over a range of grain sizes (at the same applied stress and temperature) are necessary. Such a study would enable determination of the inverse grain size exponent, p, in Equation 1. Although theoretical analyses of IRC have concluded that the stress dependency of creep rate, n, may be either 2 [13–15] or 1 [11], depending on whether or not boundary dislocation density is assumed to be (linearly) dependent on σ_{app}, all are in agreement that $p = 1$. This feature makes the IRC mechanism distinguishable from purely diffusional mechanisms in which $p = 2$ or 3 (for Nabarro–Herring or Coble creep, respectively). Unfortunately, another rate-controlling mechanism, unaccommodated grain-boundary sliding (GBS), also predicts the stress and grain-size dependency of the creep rate to be 2 and 1, respectively [10]. One would, however, expect the microstructure of a material crept via unaccommodated GBS to differ from that of a material crept via IRC; i.e. cavitation would not be expected in the latter.

Attempts to relate the time-to-failure to the steady-state creep behaviour have resulted in several empirical relation schemes. The Monkman–Grant relationship, given by

$$t_f \dot{\varepsilon}_{ss}^m = C \quad (3)$$

has been used with some success to make these correlations for various types of ceramics. It may be used to define a limiting creep rate (and in conjunction with Equation 1, a limiting σ_{app}) necessary to ensure specimen lifetime. Significant differences exist between the rupture behaviour of single filaments and bundles of the alumina–zirconia fibre (at 1200 °C), as shown in Fig. 10. Note that, for a given creep rate (or applied stress), the bundle samples exhibit longer lifetimes with the effect becoming more pronounced at higher creep rates (higher stresses).

In comparing the creep behaviour of these alumina-based fibres to other ceramic fibres, the steady-state creep rates are found to be 2 to 3 orders of magnitude greater than those obtained for Nicalon at similar temperatures [6]. The polycrystalline oxide fibres are also inferior to the Nicalon fibres in stress-rupture characteristics at these temperatures [17].

5. Conclusion

Techniques were developed for testing both single filaments and bundles of ceramic fibres in creep rupture. Preliminary investigations of an alumina and an alumina–zirconia fibre indicate that, at applied stresses from 50–150 MPa and temperatures of 1150–1250 °C, steady-state creep rates of the alumina–zirconia fibre ranged from 4.12×10^{-8}–$7.70 \times 10^{-6}\,\mathrm{s^{-1}}$. At a given applied stress, at 1200 °C, creep rates for the alumina fibre were 2–10 times greater than those of the alumina–zirconia fibre. Stress exponents for both fibres ranged from 1.2–2.8, while the apparent activation energy for creep of bundles of the alumina–zirconia fibre was determined to be 648 $\pm$ 100 $\mathrm{kJ\,mol^{-1}}$. The mechanism controlling steady-state creep of these alumina-based fibres is suggested to be interface-reaction-controlled diffusional creep.

Investigations are continuing in order to (1) validate the proposed rate controlling mechanism, (2) determine the mechanism(s) inhibiting creep deformation in the alumina–zirconia material, and (3) determine the events leading to both fibre and bundle failure.

References

1. G. SIMON and A. R. BUNSELL, *J. Mater. Sci. Lett.* **2** (1983) 80.
2. *Idem, J. Mater. Sci.* **19** (1984) 3658.
3. A. R. BUNSELL and G. SIMON, *Compos. Sci. Technol.* **27** (1986) 157.
4. D. D. JOHNSON, A. R. HOLTZ and M. F. GRETHER, *Ceram. Engng Sci. Proc.* **8** (1987) 744.
5. K. JAKUS and V. TULLURI, *Ceram. Engng. Sci. Proc.* **10** (1989) 1338.
6. R. E. TRESSLER and N. Jia, in "Projects Within the Center for Advanced Materials," Report to Gas Research Institute, edited by J. R. Hellmann and B. K. Kennedy, NIJS No. PB89-142624, pp. 234–52, 1987–1988.
7. J. C. ROMINE, *Ceram. Engng Sci. Proc.* **8** (1987) 755.
8. B. B. GHATE, D. P. H. HASSELMAN and R. M. SPRIGGS, *Bull. Amer. Ceram. Soc.* **52** (1973) 670.
9. K. JAKUS and V. TULLURI, *Ceram. Engng Sci. Proc.* **10** (1989) 1338.
10. W. R. CANNON and T. G. LANGDON, *J. Mater. Sci.* **18** (1983) 1.
11. A. H. CHOKSHI and J. R. PORTER, *Ibid.* **21** (1986) 705.
12. F. WAKAI, T. IGA and T. NAGANO, *J. Ceram. Soc. Jpn Inter. Ed.* **96** (1988) 1176.
13. B. BURTON, *Mater. Sci. Engng* **10** (1972) 9.
14. E. ARZT, M. F. ASHBY and R. A. VERRALL, *Acta. Metall.* **31** (1983) 1977.
15. E. ARZT, *J. Phys.* **C4** (1985) 627.
16. Y. IKUMA and R. S. GORDON, in "Surfaces and Interfaces in Ceramic and Ceramic-Metal Systems", edited by J. Pask and A. Evans (Plenum Press, NY, 1981) pp. 283–93.
17. R. E. TRESSLER and D. J. PYSHER, in "Proceedings of CIMTEC 7", 7th World Ceramics Congress, Montecatini Terme, Italy, June 1990.

Received 6 August 1990
and accepted 12 February 1991